SCIPEDIA Revista Internacional de Métodos Numéricos para Cálculo y Diseño en Ingeniería

Revista Internacional Métodos numéricos para cálculo y diseño en ingeniería RIMNI

UNIVERSITAT POLITÈCNICA DE CATALUNYA BARCELONATECH In cooperation with CIMNE

Research of an EPB shield pressure and depth prediction model based on deep neural network and its control device

Jiacheng Shao[12], Jingxiu Ling[123], Rongchang Zhang[12], Xiaoyuan Cheng[12], Hao Zhang[3]

1 The Key Laboratory of Intelligent Machining Technology and Equipment, Fujian University of Technology, China

2 School of Mechanical and Automotive Engineering, Fujian University of Technology, China

3 CSCEC Strait Construction and Development Co, Ltd, Fuzhou, China

Abstract

Based on the construction data of Fuzhou Metro Line 4 in Fujian Province, China, this paper proposes a soil pressure prediction model that combines Long Short-Term Memory (LSTM) and Particle Swarm Optimization (PSO). The values of Mean Absolute Error, Mean Squared Error, and Coefficient of Determination are 0.007MPa, 0.007%, and 0.93, respectively, indicating an improvement in accuracy.Wang-Mendel algorithm is used to establish fuzzy rules. The Mean Absolute Error and Mean Squared Error of the rotating speed of the screw machine are 0.065rpm and 1.528%, and the Coefficient of Determination is 0.82. The calculation accuracy of this algorithm is high.A set of knob intelligent control device is developed.The Mean Absolute Error and Mean Squared Error of 0.015rpm and 0.392%, respectively, and the Coefficient of Determination of 0.95, indicating a small execution error of the device. This paper provides a new and effective method for the control of EPB shield pressure.

OPEN ACCESS

Published: 19/01/2024

Accepted: 03/01/2024

DOI: 10.23967/j.rimni.2024.01.004

Keywords:
EPB
Soil pressure prediction
LSTM
PSO

1. Introduction

EPB uses dynamic balance control of water and soil pressure in front of the excavation face to avoid surface deformation. Soil pressure control involves multi-field coupling of multiple subsystems, such as the cutterhead system, propulsion system, and screw conveyor system, as well as the comprehensive effects of multiple factors such as excavation parameters and muck properties. Therefore, establishing a soil pressure control model is one of the key challenges in shield tunneling technology.Currently, the control of soil pressure in shield tunneling is generally achieved through two approaches: the establishment of a mechanism model based on mathematical and physical relationships or the use of intelligent methods such as neural networks based on on-site data. With an accurate model, it is possible to make correct predictions of future states based on past and current conditions and then optimize and control controllable variables to achieve effective control of soil pressure.

Previous studies have conducted extensive research on earth pressure balance.Hu et al. used electro-hydraulic proportional control technology to control the propulsion speed or screw machine speed in real-time on a simulation experimental platform, demonstrating that controlling the screw machine speed can achieve control of soil pressure. Based on this, they further used self-tuning PID to regulate the screw conveyor speed to achieve control of soil pressure [1]. Wang and Fu derived three basic equations for EPB shield based on model test results, and then obtained two total balance equations for EPB shield, establishing a mathematical model for EPB shield excavation [2]. Wang et al. proposed a soil pressure balance control system based on the feedback of advance speed and soil pressure, building upon previous mechanism models [3]. In recent years, neural networks have been widely used in soil pressure prediction and shield tunneling. Yeh pioneered the use of neural networks in the control of soil pressure by using a backpropagation neural network to establish a control model with the current soil pressure, advancing speed, screw conveyor speed, next moment advancing speed, next moment screw conveyor speed as inputs and next moment soil pressure as output [4]. Wei et al. combined Monte Carlo method and BP neural network model to predict the TBM's advancing speed [5]. Gao et al. used three types of recurrent neural networks (RNNs) to process real-time prediction data based on on-site TBM operating parameters, and showed that the three proposed RNN-based predictors outperformed classical regression models [6]. Liu et al. developed a long short-term memory (LSTM) network based on a global attention mechanism to predict the lithology of the excavation face [7]. Cachim and Bezuijen used a multi-layer feedforward artificial neural network to predict the cutterhead torque of an EPB-TBM, and used a time-series neural network to predict the torque as a function of the measured torque and injected foam volume at the previous time step [8]. Song et al. proposed a time series segmentation method based on fuzzy c-means clustering for TBM time series data [9]. Shi et al. proposed a new clustering algorithm based on support vector regression and fuzzy c-means algorithm (SVR-FCM) [10]. Sun et al. developed a prediction model based on integrated heterogeneous in-situ data using data-driven techniques. This method was applied in the field of non-homogeneous tunnel boring machine, which not only accurately predicted the dynamic characteristics of the load, but also accurately estimated the statistical characteristics of the load [11].

Some scholars have made research on control and particle swarm optimization. Wen et al. proposed a soil discharge

Correspondence: Jiacheng Shao (), Jingxiu Ling (ljxyxj@fjut.edu.cn).

prediction method based on an adaptive adjustment strategy and parameters to achieve optimal regression. The study analyzed the factors affecting soil flow data models using actual engineering data and found that the screw conveyor speed and total thrust were the main factors affecting the soil flow rate [12]. Liu et al. proposed an optimized control method for earth pressure based on ADHDP, which realized the online autonomous learning and adaptive control of shield tunneling chamber pressure [13]. Zhang used artificial experience to train and learn the membership functions and fuzzy rule parameters of a fuzzy system using neural networks. They established an ANFIS model for predicting the soil pressure in the shield tunneling machine and used genetic algorithms for optimizing control [14]. Zhu used a fuzzy PID control algorithm to control the factors that affect the earth pressure, and verified the correctness of the algorithm through experimental simulation [15]. Li and Gong proposed a model predictive control (MPC) system for predicting and controlling mud pressure balance during construction. The system consists of a diagonal recurrent neural network (DRNN), an optimizer that generates optimal air pressure and slurry level based on multi-step prediction, and an evolved particle swarm optimization (EPSO) algorithm. It can effectively adjust the mud circulation and air pressure maintenance system according to geological conditions [16]. Li and Li used a BP neural network for prediction and adopted the PSO algorithm to calculate the balanced control of the screw conveyor speed required for the next moment[17]. Zhang et al. proposed a method for controlling the shield tunneling machine's earth pressure using a fuzzy PID control approach based on a mechanistic model. The method was compared with the traditional PID control method, and the results showed that the proposed approach was more effective [18]. Yang developed a PSO-BP model for predicting the soil pressure in the tunnel and obtained the relationship between the predicted soil pressure and the screw conveyor speed using polynomial fitting to achieve control of soil pressure [19].

After reviewing the research status above, it was found that the input parameters considered in the mechanism control model are limited, and it is difficult to obtain some parameters such as the screw conveyor excavation efficiency and the tangential modulus of deformation of the spoil. In intelligent control models such as neural networks, after the pressure prediction model is obtained, the corresponding screw conveyor speed needs to be calculated using algorithms such as PSO and genetic algorithms, which is time-consuming. In order to facilitate engineering application, this paper will establish a PSO-LSTM deep neural network prediction model, use the WM algorithm to establish fuzzy rules for easy calculation, and develop an intelligent control device. The feasibility of the device will be verified through actual engineering data.

2. Theoretical background

2.1 LSTM neural network

In many studies that use neural networks, it is necessary to deal with sequential data and utilize its historical information. Therefore, it is necessary to enable neural networks to have memory function. The long short-term memory (LSTM) network is selected, and its structure is shown in Figure 1.

LSTM network introduces an internal state c_t specifically for the linear recurrent information transfer, as shown in Eq.(1). At the same time, it transfers the non-linear output information to the external state h_t of the hidden layer, as shown in Eq.(2):

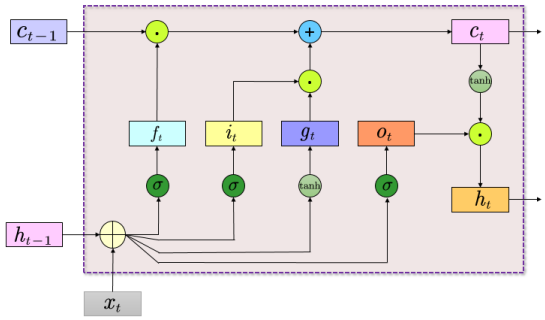

Figure 1. LSTM network structure

$$c_t = f_t \odot c_{t-1} + i_t \odot g_t \tag{1}$$

$$h_t = o_t \odot \tag{2}$$

In Eqs.(1) and (2), c_t represents, at each time step t, the internal state c_t stores the historical information from the beginning up to the current time step; ⊙denotes element-wise multiplication of vectors; c_{t-1} is the memory cell from the previous time step; h_t is both the current time step t's output of the hidden layer and the input of the hidden layer for the next time step $t+1$; $\tanh(x)$ is the activation function, defined by Eq.(3), with a range of $(-1, 1)$

$$\tanh = \frac{\exp(x) - \exp(-x)}{\exp(x) + \exp(-x)} \tag{3}$$

where g_t is the candidate state obtained through a nonlinear function, as shown in Eq.(4)

$$g_t = \tanh\left(W_{ig}x_t + b_{ig} + W_{hg}h_{t-1} + b_{hg}\right) \tag{4}$$

where $f_t \in [0, 1]$ is the forget gate, which controls how much information from the previous internal state c_{t-1} should be forgotten, as shown in Eq.(5)

$$i_t = \sigma\left(W_{ii}x_t + b_{ii} + W_{hi}h_{t-1} + b_{hi}\right) \tag{5}$$

where $i_t \in [0, 1]$ represents the input gate, which controls how much information the candidate state g_t should store at the current time step, as shown in Eq.(6)

$$f_t = \sigma(W_{if}x_t + b_{if} + W_{hf}h_{t-1} + b_{hf}) \tag{6}$$

where $o_t \in [0, 1]$ represents the output gate, which controls how much information from the current internal state c_t is output to the external state h_t, as shown in Eq.(7)

$$o_t = \sigma\left(W_{io}x_t + b_{io} + W_{ho}h_{t-1} + b_{ho}\right) \tag{7}$$

where x_t is the input at the current time step, and h_{t-1} is the external state at the previous time step; w_{ii}, b_{ii}, w_{if}, b_{if}, w_{io}, b_{io}, w_{ig}, b_{ig} are parameter matrices for the linear transformation of input x_t; w_{hi}, b_{hi}, w_{hf}, b_{hf}, w_{ho}, b_{ho}, w_{hg}, b_{hg} are the parameter matrices for the linear transformation of h_{t-1}; $\sigma(x)$ is the activation function, whose range is $(0, 1)$, and is defined by Eq.(8)

$$\sigma(x) = \frac{1}{1+\exp(-x)} \tag{8}$$

The computation process of LSTM neural network is as follows:

(1) Calculate three gates and a candidate state g_t using the current input x_t and the previous external state h_{t-1}.

(2) Update the memory cell c_t through the forget gate f_t and the input gate o_t.

(3) Use the output gate o_t to pass the information from the internal state to the external state h_t.

2.2 PSO (Particle Swarm Optimization)

Particle Swarm Optimization (PSO) is mainly inspired by the collective behavior of bird flocking and the cognitive mechanism of humans.Assuming the position of particle i randomly placed in the search space is $x_i = (x_1, x_2, ..., x_{id}, ..., x_{in})$ and its velocity is $v_i = (v_{i1}, v_{i2}, ..., v_{id}, ..., v_{in})$, then the individual best value of the particle based on the fitness function is $P_i = (P_{i1}, P_{i2}, ..., P_{id}, ..., P_{in})$, and the global best value of the swarm is $P_{gi} = (P_{g1}, P_{g2}, ..., P_{gd}, ..., P_{gn})$. The evolution equations for the particle swarm algorithm are given by Eqs.(9) and (10)

$$V_{id}^{k+1} = \omega V_{id}^{k} + c_1 r_1 (P_{id}^{k} - X_{id}^{k}) + c_2 r_2 (P_{gd}^{k} - X_{gd}^{k}) \tag{9}$$

$$X_{id}^{k+1} = X_{id}^{k} + V_{id}^{k+1} \tag{10}$$

where, ω is the weight coefficient: $d = 1, 2, 3...N$; k is the current iteration number; c_1, c_2, r_1, r_2 are non-negative constants randomly distributed in $[0, 1]$; to avoid large-scale blind search, the range of particle positions and velocities are limited to $[-X_{\max}, X_{\max}]$ and $[-V_{\max}, V_{\max}]$, respectively.

In this paper, PSO algorithm is mainly used to optimize the hyperparameters in the soil pressure prediction model. Therefore, the error between the predicted values obtained by the prediction model and the actual values is used as a reference value for the fitness function, and the optimization goal is to find the best combination of hyperparameters for the deep neural network. The relationship between the model to be optimized and the optimization goal can be expressed as Eq.(11):

$$loss_{\min} = \frac{\sum (y_{\text{test}} - y_{\text{true}})^2}{N_{\text{test}}} \tag{11}$$

where y_{test} is the predicted result of the model; y_{true} is the actual value; N_{test} is the number of test samples selected.

The process of optimizing the prediction model using PSO can be summarized as follows:

(1) Initialize PSO parameters and set initial values for hyperparameters of the deep neural network prediction model. Calculate the initial position for each particle, denoted as PBest, and set the best value in PBest as the global optimal value gBest.

(2) Calculate the fitness value of the prediction model by using the error between the predicted values obtained by each particle and the actual values, and record the current particle position and corresponding fitness function value.

(3) Compare the fitness value of the particle with the best fitness value it has reached, update the particle's velocity and position, and optimize.

(4) If the number of iterations is not completed, return to step 2 to continue the operation, and finally obtain the globally optimal hyperparameter combination.

2.3 Wang-Mendel algorithm

The Wang-Mendel (WM) method proposed by Wang and Mendel can effectively generate fuzzy rules from sample data [20]. This method partitions the input space into fuzzy regions and then uses a lookup table to extract rules for each fuzzy subspace. The WM method does not require repeated learning and can use a large amount of input-output data to obtain a complete fuzzy rule base that covers the entire input domain [21]. The WM method has become a classic method for fuzzy rule generation and has been widely used in various applications [22].

Therefore, in this study, the WM (Wang-Mendel) algorithm was used to establish a fuzzy rule base, which mainly includes three steps: rule extraction, rule merging, and rule inference [21].

Rule extraction refers to extracting fuzzy rules from input factor data. Firstly, the input factors x_j should be divided into m_j fuzzy subsets. In this paper, the input data is in the form of n inputs and one output, which can be expressed as $(x^{(I)}, y)$, $I = 1, 2, ..., n$. Where $x^{(I)} \in R^n$ represents the input factors and $y \in R$ represents the output factor. The input factor data is fuzzified and divided into L fuzzy subspaces using the triangular membership function Eq.(14), as shown in Eq.(13). Then, one rule can be extracted from each of the k data points, as shown in Eq.(12). In this way, k rules are obtained

$$if\ \mathrm{x}_1 \text{ is } A_1^{l_1} \text{ and} \cdots \text{and } \mathrm{x}_n \text{ is } A_n^{l_n}, \text{then y is } B^l \tag{12}$$

$$L = \prod_{j=1}^{n} m_j \tag{13}$$

$$u(y, y_c, \sigma) = \frac{\sigma - |y - y_c|}{\sigma} \tag{14}$$

$$y_c{}^l = \frac{\sum_{k=1}^{N_k} y_k^{(i)} \omega_k^{(i)}}{\sum_{k=1}^{N_k} \omega_k^{(i)}} \tag{15}$$

$$\sigma = \frac{\sum_{k=1}^{Nk} |y_k^{(i)} - y_c^l| \, \omega_k^{(i)}}{\sum_{k=1}^{Nk} \omega_k^{(i)}} \tag{16}$$

where $l = 1, ..., L$; there are m_n fuzzy sets $\{A_n^{lb} \mid l_b = 1, ..., m_n\}$ on the input domain of input factor x_n. A_n^{lb} represents the fuzzy set on input x_b with index l_d; B^l represents the fuzzy set on the output domain $U_B^l(y) = u(y, y_c^l, \sigma^l)$, where σ is the width of the fuzzy set, y_c is the center point of the fuzzy set, defined by Eqs.(15) and (16), where $y \in [y_c - \sigma, y_c + \sigma]$. l is the rule index corresponding to it in the rule base. L fuzzy sets correspond to L fuzzy rules. Then, the rules with the same premise conditions are merged, and the confidence degrees of the duplicate and

conflicting rules are calculated. By comparing the confidence degrees, the rules with low confidence are removed. Suppose there are H groups of duplicate rules, each containing N_h rules. The weight of each rule is calculated using Eq.(17). The larger the weight, the closer the rule is to the center of the fuzzy space. Then, N_h rules are merged into a single rule in the form of Eq.(12), and the reliability of the rule is calculated using Eq.(18). Finally, the reliable rules are selected and added to the rule base.

$$\omega_k^{(i)} = \prod_{j=1}^{n} U_{A_j}^{l_j}(x_j^{(i)}) \tag{17}$$

$$doc^l = 1 - \frac{\sigma^l}{\max_{k,t=1}^{N_h} |y_k^{(i)} - y_t^{(i)}|} \tag{18}$$

3. Process and analysis

3.1 Data Acquisition and Cleaning

The research data in this paper is based on the construction site of Subway Line 4 in Fuzhou City. Data is collected and saved to the database in real-time at intervals of one minute.

In the research process, the correct selection of factor data determines the correct match between the analysis object and the results. Due to the large number of excavation factor data generated by the shield machine during the excavation process, and the existence of missing values and outliers to some extent in each factor, it is necessary to clean the raw data to improve the quality of factor data.

The effectiveness of data cleaning directly affects the accuracy of subsequent data analysis and model predictions. Through investigation and monitoring of the construction site of Fuzhou Metro Line 4, based on traditional data preprocessing methods and fully considering factors such as the shield tunneling construction process, construction conditions, and the operator's habits, this article formulated the following five data cleaning principles:

(1) Based on detailed geological survey data, select shield tunneling data under the same geological conditions as the research object, excluding the influence of different geological conditions on the soil pressure caused by the shield machine.

(2) Due to the large amount of data, delete the real-time factor data corresponding to missing or abnormal values in each factor to ensure the correspondence between the data of each factor.

(3) Data corresponding to abnormal tunneling states such as stand-by, stoppage, cutterhead replacement, and mechanical failure are deleted to ensure that the data only includes those from normal tunneling processes of the shield machine.

(4) Data for monitoring factors such as horizontal deviation, front and rear mileage, mechanical and electrical parameters, and vertical deviation with values of 0 are removed.

(5) If the data of a certain factor is 0, the corresponding real-time data of other factors will be deleted to ensure the correspondence between each factor data.

After applying the above data cleaning principles, a total of 27 rings, 3525 sets of data, and 32 excavation factors were selected in the excavation factors data ranging from ring 407 to 434.

3.2 Spearman correlation analysis

In this paper, to investigate whether there is a relationship between the shield tunneling factors and the earth pressure in the cutterhead chamber, as well as the degree of correlation, it is necessary to perform a correlation analysis.Two commonly used methods for correlation analysis are the Pearson correlation coefficient and the Spearman correlation coefficient. The Pearson correlation coefficient belongs to parametric statistical methods, while the Spearman correlation coefficient belongs to non-parametric statistical methods. Therefore, it is necessary to perform normality test on the 32 data factors obtained from the previous data cleaning. This article lists the histograms and Q-Q plots of the following three excavation factors, as shown in Figures 2 to 4. As shown in the figures, some factors follow normal distribution while others do not, indicating that the Spearman correlation coefficient should be chosen for analysis.

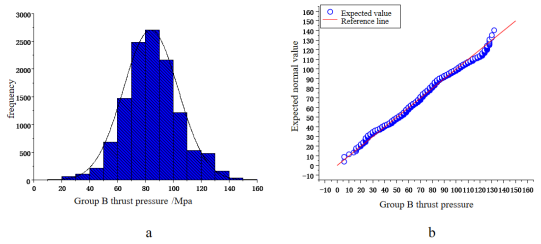

Figure 2. Boring pressure of Group B. (a) Histogram. (b) Q-Q plot

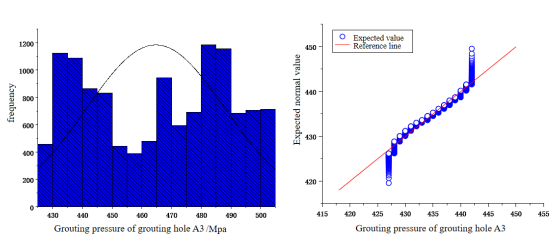

Figure 3. Grouting pressure of grouting hole A3. (a) Histogram. (b) Q-Q plot

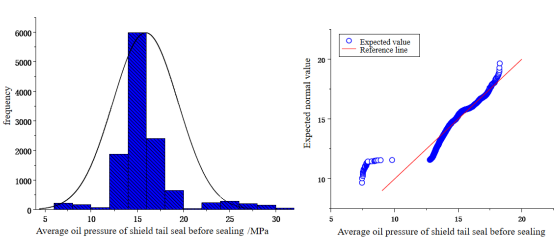

Figure 4. Average oil pressure of the tail seal before the shield closure of the front chamber. (a) Histogram. (b) Q-Q plot

The Spearman correlation coefficient, also known as the rank correlation coefficient, is calculated using the following Eq.(19):

$$r = \frac{\sum_{i=1}^{N}(R_i - \overline{R})(S_i - \overline{S})}{\left[\sum_{i=1}^{N}(R_i - \overline{R})^2 \sum_{i=1}^{N}(S_i - \overline{S})^2\right]^{\frac{1}{2}}} \quad (19)$$

where R_i and S_i represent the rank order of the observed value i; R and S are the average rank orders of x and y, respectively; N is the total number of observed values.

Apart from the factor of silo pressure, this study conducted correlation analysis between 31 other factors and silo pressure using SPSS. The results are shown in Table 1 and Figure 5. The value of the Spearman correlation coefficient r ranges from -1 to 1, where values between 0 and 1 indicate a positive correlation and values between -1 and 0 indicate a negative correlation. The absolute value of the correlation coefficient $|r|$ represents the degree of correlation between the two factors, and the correlation strength can generally be judged and described using Table 2 [23].

Table 1. Spearman correlation coefficients between tunneling factors and earth pressure for each excavation factor ID

Factor number	Factor name	Spearman correlation coefficient r	Degree of correlation
1	Advance speed (mm/min)	0.297**	Weak
2	Cutter speed (r/min)	-0.239**	Weak
3	Cutter Torque (kn.m)	0.378**	Weak
4	Total thrust (kn)	0.683**	Strong
5	Group A propulsion pressure (MPa)	0.07**	Unrelated
6	Group B propulsion pressure (MPa)	0.532**	Moderate
7	Group C propulsion pressure (MPa)	0.062**	Unrelated
8	Group D propulsion pressure (MPa)	0.151**	Unrelated
9	Group A advance displacement (mm/m)	-0.125**	Unrelated
10	Group B advance displacement (mm/m)	-0.122**	Unrelated
11	Group C advance displacement (mm/m)	-0.122**	Unrelated
12	Group D advance displacement (mm/m)	-0.129**	Unrelated
13	Grouting hole A1 grouting pressure (kn/m^2)	0.33**	Weak
14	Grouting hole A2 grouting pressure (kn/m^2)	0.049**	Unrelated
15	Grouting hole A3 grouting pressure (kn/m^2)	0.33**	Weak
16	Grouting hole A4 grouting pressure (kn/m^2)	0.025**	Unrelated
17	screw machine pressure (MPa)	0.232**	Weak
18	Screw machine torque□KN^{2}m□	0.232**	Weak
19	Screw speed□rpm□	0.326**	Weak
20	Spiral machine oil temperature (℃)	-0.188**	Unrelated
21	The average oil pressure of the shield front and tail seals (MPa)	0.278**	Weak
22	The average oil pressure of the shield tail seal of the sealed warehouse (MPa)	0.274**	Weak
23	Average pressure of foam system (MPa)	0.464**	Moderate
24	Foam Circuit Average Air Flow (L/min)	0.16**	Unrelated
25	Foam Circuit Average Liquid Flow (L/min)	-0.021	Unrelated
26	Articulation cylinder pressure (MPa)	-0.119**	Unrelated
27	Group A articulated cylinder stroke (mm/m)	-0.153**	Unrelated
28	Group B articulated cylinder stroke (mm/m)	-0.211**	Weak
29	Group C articulated cylinder stroke (mm/m)	0.165**	Unrelated
30	Group D articulated cylinder stroke (mm/m)	0.332**	Weak
31	Foam water real-time cumulative average (m^3/h)	-0.104**	Unrelated

**Exhibits significant correlation at the 0.01 level (two-tailed)

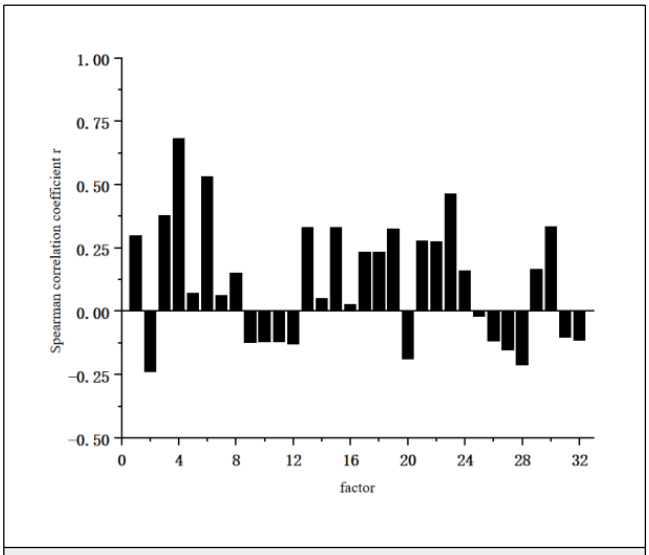

Figure 5. Results of Spearman correlation analysis

Table 2. $|r|$ Values and corresponding degrees of correlation

$\|r\|$	Correlation coefficient
(0,0.2]	Extremely Weak Correlation/Unrelated
(0.2,0.4]	Weak Correlation
(0.4,0.6]	Moderate Correlation
(0.6,0.8]	Strong Correlation
(0.8,1]	Extremely Strong Correlation

The correlation between total thrust and soil pressure is strongly correlated. The average pressure of the foam system and the push pressure of group B have a moderate correlation. The correlation between cutterhead torque, advance speed, cutterhead speed, grouting hole A1 grouting pressure, grouting hole A3 grouting pressure, screw conveyor pressure, screw conveyor torque, screw conveyor speed, average oil pressure of the front shield tail seal, average oil pressure of the rear shield tail seal, the stroke of the hinge oil cylinder of group B and group D have a weak correlation with soil pressure. Other factors have a very weak correlation and can be considered to have no correlation with soil pressure.

Therefore, this study finally determined 15 excavation factors including total thrust, B-group advance pressure, foam system average pressure, cutterhead torque, advance speed, cutterhead speed, grouting hole A1 grouting pressure, grouting hole A3 grouting pressure, screw conveyor pressure, screw conveyor torque, screw conveyor speed, average oil pressure of shield tail sealing at front chamber, average oil pressure of shield tail sealing at rear chamber, B-group articulated oil cylinder stroke, and D-group articulated oil cylinder stroke as inputs for the neural network prediction model.

3.3 Evaluation indicators

The evaluation indicators selected in this paper are mean absolute error (M_{AE}), mean squared error (M_{SE}), and coefficient of determination (R^2). The mean absolute error (M_{AE}) is used in this paper to reflect the error between the actual and predicted values, and its equation is shown in Eq.(20). The mean squared error (M_{SE}) is used to evaluate the degree of data variation, and the smaller the value, the better the predictive model's ability to accurately describe the data, as shown in Eq.(21) [24]. The coefficient of determination R^2 is used to evaluate the goodness-of-fit of a regression model. The closer its value is to 1, the better the performance of the model, as shown in Eq.(22)

$$M_{AE} = \frac{1}{n}\sum_{i=1}^{n} | \hat{y}_i - y_i | \quad (20)$$

$$M_{SE} = \frac{1}{n}\sum_{i=1}^{n} (y_i - \hat{y}_i)^2 \quad (21)$$

$$R^2 = 1 - \frac{\sum_i (\bar{y}_i - \hat{y}_i)^2}{\sum_i (y_i - \bar{y}_i)^2} \quad (22)$$

where n represents the sample size; $\hat{y}_i$ represents the predicted value; y_i represents the actual value; and $\bar{y}_i$ represents the mean value.

3.4 Model training

This paper builds an LSTM deep neural network prediction model using PyTorch deep learning framework, based on mini-batch gradient descent method and further optimized by Adam algorithm. In order to improve the accuracy of the LSTM prediction model, PSO is used to optimize LSTM parameters, and a PSO-BP prediction model is constructed using the classical BP neural network for comparison.The loss function of the prediction model is the root mean square error (RMSE) loss function. The training process is iteratively trained using the training set, and the prediction results are compared and analyzed using the test set. The hyperparameters of the four comparative models are tuned by parameter tuning, as shown in Table 3.

Table 3. Parameter tuning of four comparative models

Model parameters	Learning_rate	Lstm_layers	Hidden_size	Batch_size
LSTM	0.001	3	52	612
BP	0.001	2	62	640
PSO-LSTM	0.005	3	46	1024
PSO-BP	0.001	3	48	820

According to Figure 6 and Table 4, it can be seen that compared to the BP prediction model, the LSTM prediction model has reduced M_{AE} from 0.015 MPa to 0.011 MPa by 26.7%, reduced M_{SE} from 0.028% to 0.015% by 46.4%, and increased the absolute coefficient R^2 from 0.75 to 0.87 by 16%. It can be seen that the LSTM prediction model is better than the BP prediction model in predicting the pressure of the soil bin.Compared with PSO-BP, PSO-LSTM reduced M_{AE} from 0.010 MPa to 0.007 MPa, a decrease of 30%, reduced M_{SE} from 0.018% to 0.007%, a decrease of 61.1%, and increased R^2 from 0.84 to 0.93, an improvement of 10.7%. It can be seen that PSO-optimized LSTM prediction model performs better than PSO-optimized BP prediction model in predicting the pressure in the soil bin.Compared with the LSTM prediction model, the PSO-optimized model has reduced M_{AE} from 0.011 MPa to 0.007 MPa, a decrease of 36.4%, M_{SE} from 0.015% to 0.007%, a decrease of 53.3%, and R^2 from 0.87 to 0.93, an increase of 6.9%, indicating that using PSO to optimize the LSTM prediction model can improve its prediction accuracy.

Table 4. Comparison results

Test group	M_{AE} (MPa)	M_{SE} (%)	R^2
PSO-BP	0.010	0.018	0.84
PSO-LSTM	0.007	0.007	0.93
LSTM	0.011	0.015	0.87
BP	0.015	0.028	0.75

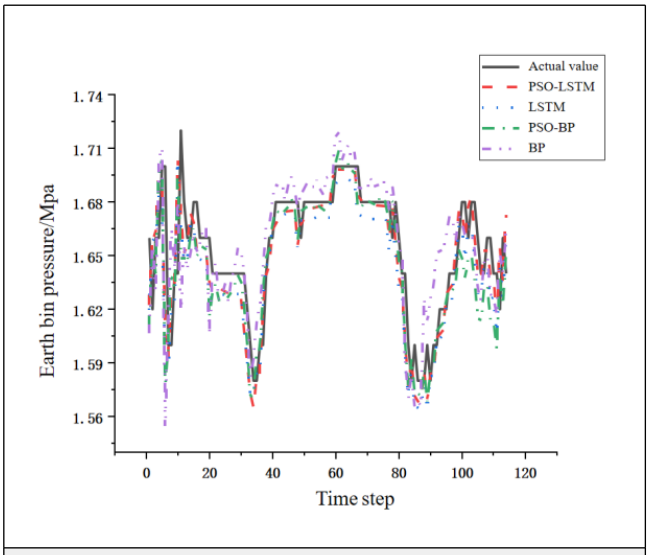

Figure 6. Graphs of the four comparative models

3.5 Fuzzy control

In order to achieve the application of intelligent control of shield machines in practical engineering, this paper needs to obtain the corresponding relationship between the soil pressure and the screw machine speed. As the six factors of advancing speed, cutterhead speed, total thrust, cutterhead torque, screw machine speed, and soil pressure can be obtained from the monitoring room of a shield machine, historical data of these six factors from ring 407 to 433 were selected as the training set, and the data from ring 434 was used as the test set to construct a 5-input single-output fuzzy control rule.

The maximum and minimum values of each factor are taken as the domain range, and the triangular membership function is used to automatically partition the fuzzy set based on the specified number of partition intervals for each factor. The data is then fuzzified, and the membership degree of each data point on the fuzzy set is calculated. The highest membership degree value is selected as the basis for a fuzzy rule. Due to the large number of repeated rules in these rules, their confidence levels are calculated separately and filtered to establish a fuzzy rule base.

The predicted value of the 434th ring shield pressure obtained by the LSTM prediction model, together with the real-time read push speed, cutterhead speed, total thrust, and cutterhead torque that can be obtained from the shield machine monitoring room, are used as inputs to the fuzzy rules. The corresponding target value of the screw conveyor speed is obtained, as shown in Figure 7.

According to Table 5, the errors between the extracted fuzzy rules for screw machine speed and the actual values, obtained through the WM algorithm from historical data, are 0.065rpm for M_{AE}, 1.528% for M_{SE}, and 0.82 for absolute coefficient R^2, indicating that the accuracy of the fuzzy rule base established by the algorithm is relatively high and basically meets the requirements.

Table 5. Evaluation indicators of WM calculated values and motor operation values

Evaluation index	M_{AE} (rpm)	M_{SE} (%)	R^2
Fuzzy rule calculation value	0.065	1.528	0.82

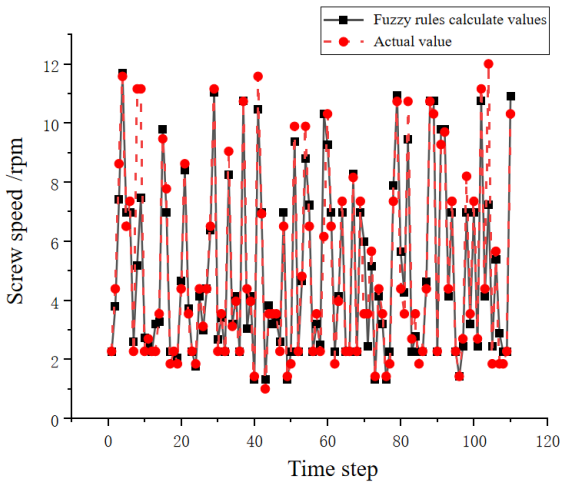

Figure 7. Graph of the variation in screw machine speed

3.6 intelligent control device

To achieve precise control of the screw conveyor, it is essentially precise control of the drive motor. Based on the actual situation of the Fuzhou Metro Line 4 shield machine control room, this paper uses an Arduino main control board, Simple FOC to drive a BLDC brushless DC motor, and an AS5600 magnetic encoder as the motor's position sensor to create an intelligent control device for the shield screw machine control knob, as shown in Figure 8.

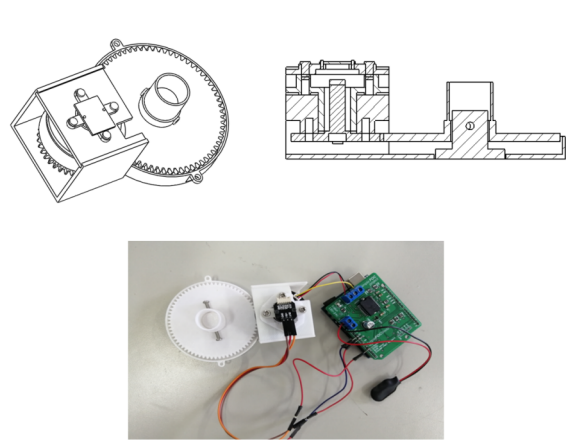

Figure 8. Intelligent control device for the screw machine speed control knob

The working principle of the intelligent control device for the shield spiral conveyor is as follows: When the PC sends a position target command to the Arduino main control board through USB serial communication, the Simple FOC drives the BLDC brushless DC motor to start. The motor gear fixed on the top of the BLDC brushless DC motor rotates, and through the gear meshing with the knob gear, the motor torque is transmitted to the knob gear, thereby driving the speed knob of the spiral conveyor fixed by screws under the knob gear. The AS5600 magnetic sensor obtains the position data of the BLDC brushless DC motor rotation by fixing a radial magnet on the top of the cylindrical center of the motor gear, feeds it back to the Arduino main control board through I2C and transmits it to the PC through USB serial communication. The brushless DC motor stops rotating when it reaches the target position.

The intelligent control device established in this article mainly includes two parts: hardware and software. The key to establishing the overall control program is to realize the communication between Python and Arduino microcontroller. The structure of the overall control program established in this article is shown in Figure 9, and the control flow of the overall program is shown in Figure 10.

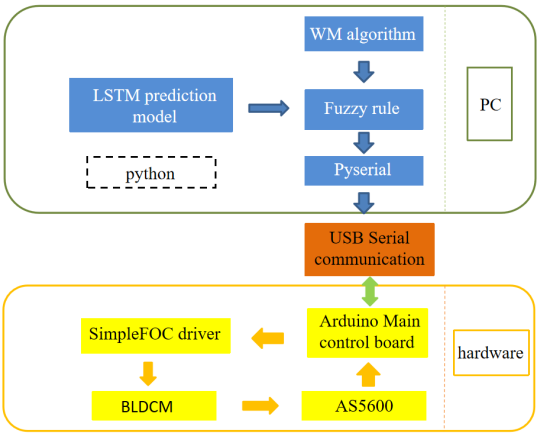

Figure 9. Structure of the central control program

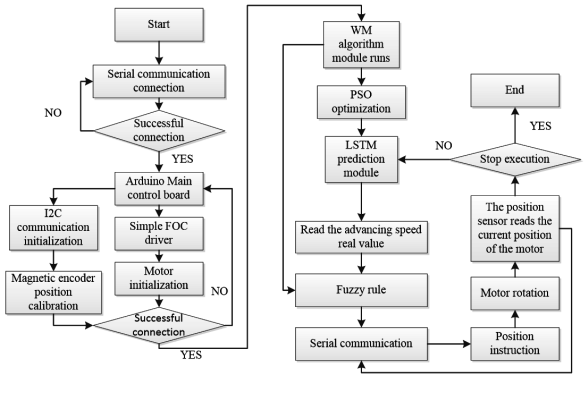

Figure 10. Overall program control flow

The performance of the intelligent control device was validated using actual data from the 434-ring earth pressure balance shield machine of Fuzhou Metro Line 4. The predicted silo pressure values obtained from the PSO-LSTM model were used as inputs to the fuzzy rules, and the corresponding spiral machine speed target control values were obtained. The results are shown in Figure 11.

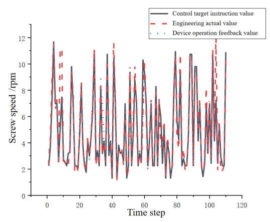

Figure 11. Comparison between control target instructions and actual spiral machine speed and feedback values of the control device

According to Table 6, the M_{AE} and M_{SE} errors of the fuzzy rules calculated from the WM algorithm, based on the PSO-LSTM model's predicted value of silo pressure, and the corresponding spiral speed value compared with the actual spiral speed value are 0.065 rpm and 1.528%, respectively. The absolute coefficient R^2 can reach 0.82, indicating that the calculation effect is good and basically meets the requirements. Comparing the real-time data of the motor's rotation position feedback by the intelligent control device's magnetic encoder and the control target instruction value, there are M_{AE} and M_{SE} errors of 0.015 rpm and 0.392%, respectively, between the effect executed by the intelligent control device and the target input instruction. The absolute coefficient R^2 is 0.95, indicating that the execution error of the device is small. Therefore, the feasibility and reliability of the device have been verified.

Table 6. Evaluation indicators of the comparison between the control target instruction, device operation feedback value, and actual engineering data

Contrast	M_{AE} **(rpm)**	M_{SE} **(%)**	R^2
Control target command value	0.065	1.528	0.82
Device operation feedback value	0.015	0.392	0.95

4. Conclusion

This paper relies on the construction site data of Fuzhou Metro Line 4 in Fujian Province, China, and proposes a soil bin pressure prediction model combining LSTM and PSO. Its mean absolute error, mean squared error, and coefficient of determination values are 0.007MPa, 0.007%, and 0.93, respectively, which show improved accuracy compared to other prediction models.Meanwhile, the Wang-Mendel algorithm was used to extract fuzzy rules from historical data. The mean absolute error and mean square error of the rotating speed of the screw machine were 0.065rpm and 1.528%, and the coefficient of determination was 0.82, indicating that the fuzzy rule base established by the algorithm had high calculation accuracy.The development of an intelligent control device aimed at controlling the screw machine speed knob showed the mean absolute error and mean square error of 0.015rpm and 0.392%, respectively, with the absolute coefficient of 0.95, indicating that the device had low execution error. The research content of this paper is reliable and provides a new and effective method for controlling the EPB soil pressure.

Acknowledgments

This work was supported by the Natural Science Foundation of Fujian Province (Grant No.2022J01390), the China Postdoctoral Science Foundation (Grant No.2020M671956) ,Fujian Province Foreign Cooperation Industrialization Project(Grant No.2021I1006) and Fujian Province technology innovation key research and industrialization projects(Grant No.2023XQ002）

References

[1] Hu G., Gong G.-F., Yang H. Realization of earth pressure balance for shield tunnelling machine (in Chinese). Journal of Zhejiang University (Engineering Science), 2006(05):874-877, 2006.

[2] Wang H., Fu D. A mathematical model and the related parameters for EPB shield tunneling (in Chinese). China Civil Engineering Journal, 2006(09):86-90, 2006.

[3] Wang L., Gong G.-F., Yang H., Hou D. Earth pressure balance control based on feedforward-feedback compound control (in Chinese). Journal of Central South University (Science and Technology), 44(07):2726-2735, 2013.

[4] Yeh I.C. Application of neural networks to automatic soil pressure balance control for shield tunneling. Automation in Construction, 5(5):421-426, 1997.

[5] Wei M., Wang Z., Wang X. et al. Prediction of TBM penetration rate based on Monte Carlo-BP neural network. Neural Comput. & Applic., 33:603–611, 2021.

[6] Gao X., Shi M., Song X., Zhang C., Zhang h. Recurrent neural networks for real-time prediction of TBM operating parameters. Automation in Construction, 98:225-235, 2019. https://doi.org/10.1016/j.autcon.2018.11.013

[7] Liu z., Li l., Fang x., Qi w., Shen j., Zhou H., Zhang Y. Hard-rock tunnel lithology prediction with TBM construction big data using a global-attention-mechanism-based LSTM network. Automation in Construction, 125, 103647, 2021. https://doi.org/10.1016/j.autcon.2021.103647

[8] Cachim P., Bezuijen A. Modelling the torque with artificial neural networks on a tunnel boring machine. KSCE J. Civ. Eng., 23:4529–4537, 2019. https://doi.org/10.1007/s12205-019-0302-0

[9] Song X., Shi M., Wu J., Sun W. A new fuzzy c-means clustering-based time series segmentation approach and its application on tunnel boring machine analysis. Mechanical Systems and Signal Processing, 133, 106279, 2019. https://doi.org/10.1016/j.ymssp.2019.106279

[10] Shi M., Zhang T., Zhang L., Sun W., Song X. A fuzzy c-means algorithm based on the relationship among attributes of data and its application in tunnel boring machine. Knowledge-Based Systems, 191, 105229, 2020.

[11] Sun W., Shi M., Zhang C., Zhao J., Song X. Dynamic load prediction of tunnel boring machine (TBM) based on heterogeneous in-situ data. Automation in Construction, 92:23-34, 2018. https://doi.org/10.1016/j.autcon.2018.03.030

[12] Wen Z., Wang Z., Rong X. et al. Prediction of the amount of soil discharged by an earth pressure balanced shield machine based on feature engineering. KSCE J. Civ. Eng. 25:4868–4886, 2021.

[13] Liu X., Xu S., Huang Y. Optimal control for earth pressure balance of shield machine based on action-dependent heuristic dynamic programming. ISA Transactions, 94:28-35, 2019. https://doi.org/10.1016/j.isatra.2019.04.007.

[14] Zhang Y. Multi-point earth pressure prediction and optimal control method for EPB shield capsule (in Chinese). Dalian University of Technology, Master's Theses, 2011. http://kns.cnki.net/I =OVERSEA&v=E60D5TP9SJIrmFT2djX4fI-7vn5r7A38JG9gv1pEeVHMLVKMZHtlrPs6SWS3gBa0

[15] Zhu H.-T. Research of earth pressure balance control of shield machine based on the Fuzzy PID algorithm (in Chinese). Chinese Hydraulics & Pneumatics, 262(06):103-107, 2013.

[16] Li X., Gong G. Predictive control of slurry pressure balance in shield tunneling using diagonal recurrent neural network and evolved particle swarm optimization. Automation in Construction, 107, 102928, 2019.

[17] Li Q., Li J. Chamber earth pressure balance control for shield machine based on PSO-BP prediction model (in Chinese). Information Technology and Network Security, 37(04):94-99, 2018. DOI:10.19358/j.issn.2096-5133.2018.04.022.

[18] Zhang C., Guo J., Zhang H., Zhou Q. Research of earth pressure balance control based on the fuzzy PID (in Chinese). Journal of Shijiazhuang Tiedao University (Natural Science Edition), 32(03):82-88, 2019. DOI:10.13319/j.cnki.sjztddxxbzrb.20180024.

[19] Yang X. Intelligent prediction of in-chamber earth pressure for EPB shield and optimization of tunneling parameters based on machine learning (in Chinese). Shandong University, Master's Theses, 2022. DOI:10.27272/d.cnki.gshdu.2022.002796.

[20] Wang L.X., Mendel J.M. Generating fuzzy rules by learning from examples. IEEE Trans. Syst. Man Cybern., 22(6):1414–1427, 1992.

[21] Shen J., Li S.-Y. Extraction and application of the fuzzy control rules based on Wang-Mendel fuzzy model (in Chinese). Journal of Systems Englneering and Electronics, 336(09):1524-1528, 2007.

[22] Wang Y., Wang D., Chai T. Extract of fuzzy rules with completeness and robustness (in Chinese). Acta Autom. Sin., 36(9):1337–1342, 2010.

[23] Li K., Tian G.-F., Ma H.-W., Yang X.-Lin, Pu B.-J., Jiang Y.-C. Correlation analysis and prediction model of boring parameters of earth pressure balance shield (in Chinese). Science Technology and Engineering, 21(09):3814-3821, 2021.

[24] Yang K., Zhang Q., Zhou S. Advance rate prediction by recurrent neural networks analysis on in-situ data of tunnel boring machines (in Chinese). Mechanical Science and Technology for Aerospace Engineering, 40(6)835-839, 2021.